CHAPTER 5

Flexoelectricity and Mechanotransduction

Alexander G. Petrov
Institute of Solid State Physics, Bulgarian Academy of Sciences,
72 Tzarigradsko Chaussee, 1784 Sofia, Bulgaria

I. OVERVIEW

Flexoelectricity is a biophysical phenomenon that provides a reciprocal relationship between membrane curvature and polarization, thus enabling various membrane structures to function like mechanoreceptors. Experimental evidence of biomembrane flexoelectricity (including direct and converse flexoelectric effect) is reviewed. Mechanotransduction by flexoelectric membranes, either channel-free or channel-containing, is underlined.

II. INTRODUCTION

Flexoelectricity is a mechanoelectric property of liquid crystals similar to the piezoelectric effect in solid crystals (Meyer, 1969). In most liquid crystals, an applied electric field may induce an orientational distortion of the local

Current Topics in Membranes, Volume 58
1063-5823/07 $35.00

DOI: 10.1016/S1063-5823(06)58005-6

directors due to flexoelectricity. Conversely, any distortion of the director field will induce a macroscopic polarization within the material. In biologically manifested liquid crystal structures like biomembranes, flexoelectricity provides a reciprocal relationship between membrane curvature and polarization (Petrov, 1975), thus enabling a curvature-induced polarization (direct flexoelectric effect) or an electric field-induced curvature (converse flexoelectric effect).

On the other hand, mechanotransduction is the process by which cells convert mechanical stimuli into electrical or biochemical signals. The problem is how mechanical stresses are converted into biological signals and physiological responses [for reviews see Ingber (1997), Hamill and Martinac (2001), Orr *et al.* (2006)]. Much of the research on mechanotransduction in eukaryotes has been conducted on specialized cells whose main function is to sense and respond to mechanical stresses. These specialized cells include hair cells of the inner ear and cutaneous touchsensitive neurons. The identity of the molecules and structures that mediate mechanotransduction in these cells remains elusive. Liquid crystal physics offers an universal mechanotransducting mechanism, the flexoelectricity. A cell membrane can perform as a whole like a mechanosensor due to flexoelectricity. On the basis of the speed of mechanosensitive cells' depolarizations, however, it is almost certain that they must also possess cation channels that are mechanically gated. Since 1983 such channels have been discovered in a great variety of cells and they appear today ubiquitous (Hamill, 1983; Brehm *et al.*, 1984; Guharay and Sachs, 1984; Morris, 1990; Sachs, 1990). This far, the role of flexoelectricity is not so evident. It is the main subject of the present chapter.

III. FLEXOELECTRICITY, MEMBRANE CURVATURE, AND POLARIZATION

Flexoelectricity is well understood in liquid crystal physics (De Gennes, 1974). In the special case of a two-dimensional liquid crystal membrane, flexoelectricity means either curvature-induced membrane polarization or electric field-induced membrane curvature. In the first case (Petrov, 1975, 1999):

$$P_s = f(c_1 + c_2). \tag{1}$$

P_s is the electric polarization per unit area in C/m, c_1 and c_2 are the two principal membrane curvatures in m^{-1} (where $c_1 = 1/R_1$ and $c_2 = 1/R_2$; Fig. 1), and f is the area flexoelectric coefficient in C (Coulombs), typically a few units of electron charge. The flexocoefficient is regarded positive if polarization points outward the center of curvature (Fig. 1). This effect is manifested in liquid crystalline membrane structures because a curvature of

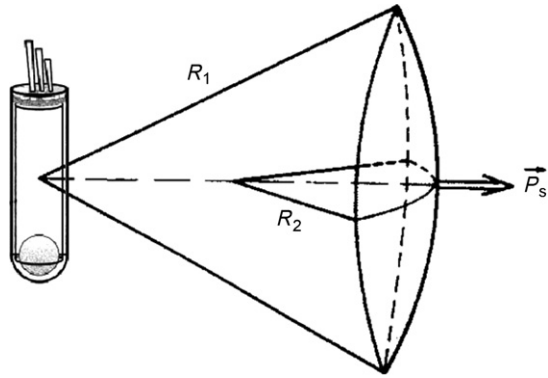

FIGURE 1 The logo of the 1st and 2nd Flexoelectric Congresses (SUNY-Buffalo, 2001 and Rice-Houston, 2003). On the right, flexoelectric (curvature-induced) polarization of a membrane P_s and sign convention about flexocoefficient f: for the case shown f will be positive. R_1 and R_2 are principal radii of membrane curvature. On the left, schematic representation of an outer hair cell (OHC) which lateral membrane is supposed to act as a flexoelectric motor (cf. Fig. 11). After Petrov *et al.* (1993; Fig. 1) with permission from the Publisher.

membrane surface leads to a liquid crystal deformation of splay type of lipids and proteins. These are otherwise oriented parallel to each other along the local membrane normal in flat state. According to the Helmholtz equation, an electric potential difference appears across a polarized surface. In view of Eq. (1), the curvature-dependent part of this potential difference is:

$$U_f = \frac{P_s}{\varepsilon_0} = \left(\frac{f}{\varepsilon_0}\right)(c_1 + c_2). \tag{2}$$

This is the expression of the direct flexoelectric effect. By measuring the total curvature and the curvature-induced potential difference, we can determine the flexoelectric coefficient of any given membrane.

Like piezoelectricity of solids, flexoelectricity is also manifested besides a direct effect [Eq. (1)] also by a converse effect, featuring electric field-induced curvature (Petrov, 1999):

$$c_1 + c_2 = \left(\frac{f}{K}\right)E, \tag{3}$$

where E is the transmembrane electric field and K is curvature elastic modulus. Eq. (3) is valid for a tension-free membrane (identically zero lateral tension), which is the case in an osmotically balanced cell.

Exploring molecular mechanisms of flexoelectricity is a central task of the liquid crystal approach in the membranology (Petrov and Derzhanski, 1976; Petrov *et al.*, 1979; Derzhanski, 1989; Petrov, 1999, 2001). Flexoelectric

coefficient can be represented as an integral over the curvature derivative of the distribution of normal component of polarization across the membrane (Petrov, 2001). Model distributions including electric monopoles, dipoles, and quadrupoles of lipids and proteins have been considered (Derzhanski, 1989; Petrov, 1999), revealing their respective contributions to the total flexocoefficient f:

$$f = f^{\mathrm{M}} + f^{\mathrm{D}} + f^{\mathrm{Q}}, \tag{4}$$

where the relative amounts of the contributions are dependent on the molecular structure of lipids/proteins and the ionic conditions of the bathing electrolyte. For a membrane that is asymmetric in its flat state, flexoelectricity will add a curvature-dependent component to its total polarization.

A. Flexoelectricity and Membrane Lipids

1. Dipole Mechanism of Flexoelectricity

In the curvature elasticity theory of lipid bilayers, a distinction is made between connected and unconnected bilayers (Petrov, 1999). The term "connected bilayer" refers to the case in which restrictions along the edges or boundaries or internal restrictions do not allow for the monolayers constituting the bilayer to slide freely one over another (or time is not enough to do so). The term "unconnected bilayer" refers to free monolayers that slide freely on each other at bending according to their relative area changes with no boundary restrictions. These two cases are considered separately:

a. Dipolar Flexoelectricity of Connected Bilayers: Blocked Lipid Exchange. In a symmetric connected bilayer, the neutral surface coincides with the mid-surface, therefore the outer monolayer (o) is expanded while the inner (i) is compressed as a whole. The change of lipid packing to more loose in the outer monolayer and to more compact in the inner one will lead to conformational changes in the headgroups and, most notably, in the structure of the polarized interfacial water. As a result, the normal components of the dipole moments per head in the two monolayers ($\mu^{\mathrm{o}}, \mu^{\mathrm{i}}$) will change, in opposite directions at that. Simultaneously, the area density of dipoles over the two interfaces will change as well. In this way, a dipole imbalance with respect to the mid-surface will arise and the symmetric bilayer will become polarized with a flexocoefficient (Petrov, 1999):

$$f^{\mathrm{DB}} = \left(\frac{\mu_0}{A_0} - \left. \frac{\mathrm{d}\mu}{\mathrm{d}A} \right|_{A_0} \right) d, \tag{5}$$

where μ is the total normal component of dipole moment per lipid head (polarized water including) and A is the area per lipid head. The superscript DB means the dipolar blocked contribution and the subscript 0 refers to the corresponding values in the flat membrane state. All values in Eq. (5) could be inferred from measurements of surface potential in lipid monolayers. For asymmetric bilayers, the sum of two corresponding expressions of the type (5) for each of the monolayers holds.

b. Dipolar Flexoelectricity of Unconnected Bilayers: Free Lipid Exchange. Unconnected bilayer bending proceeds in such a way that each monolayer is bent around its own neutral surface; relative slippage of the two monolayers is taking place so that both neutral surfaces remain unstretched and each area per lipid there equals A_0, the area over the mid-surface in flat bilayer state. If the distance from the monolayer's neutral surface to the headgroups' surface is δ_H, a residual stretching/compression will take place in the region of bilayer interfaces, numerically equal to the stretching/compression of a thinner bilayer, of thickness $2\delta_H$. Consequently, the unconnected flexoco-efficient f^{DF} of a symmetric bilayer is immediately obtainable from Eq. (5) by replacing d with $2\delta_H$. We have established an equivalence between the elastic behavior of a connected bilayer and a bilayer with both lateral and transbilayer lipid diffusion being blocked, while the case when any of these blocks is lifted is equivalent to the behavior of an unconnected bilayer (Petrov, 1999). Therefore, we can claim that f^{DF} represents the free lipid exchange contribution as well. For a bulk elastic model of the membrane $\delta_H = d/4$, that is, $f^{DF} = f^{DB}/2$. If, on the other hand, chain elasticity is vanishing, neutral surface would coincide with the surface of dipoles, that is, $\delta_H = 0$ and $f^{DF} \equiv 0$. In any case, the free dipolar contribution is less than the blocked one.

c. Flexoelectric Polarization and Transmembrane Voltage Difference. Estimation of Dipole Contribution. Eq. (5) can be rearranged as:

$$f^{DB} = -\varepsilon_0 A_0 d \left.\frac{d(\Delta V)}{dA}\right|_{A_0}, \tag{6}$$

where $\Delta V = \mu/\varepsilon_0$ and A is the surface potential for a lipid monolayer. The corresponding expression with $2\delta_H$ instead of d holds for free lipid exchange.

Equation (6) can be used to estimate f^D (Petrov, 1999). For a DPPC monolayer it follows that $f^{DB} = 1.2 \times 10^{-20}$ C. Correspondingly, f^{DF} will be about two times lower. From another set of experimental data for DPPC, we obtain $f^{DB} = 1.4 \times 10^{-20}$ C, in good agreement with the previous estimate.

Slightly higher value for f^{DB} is obtained for DPhPC: $f^{DB} = 1.7 \times 10^{-20}$ C. From the same work, it can be inferred that adsorption of PEG on DPhPC monolayers or introduction of PEG-grafted lipids in the monolayer leads to the appearance of extended ranges with an opposite sign of the surface potential derivative: $d(\Delta V)/dA > 0$. This means, according to Eq. (6), that PEG-lipids can reverse the sign of dipolar flexocoefficient from positive to negative.

2. Monopole Mechanisms of Flexoelectricity

If the lipid molecules comprising a BLM are electrically charged (with partial charge per head βe), two separate situations may be considered leading to different flexoelectric coefficients.

a. Detailed Electric Neutrality. If, after curving, each membrane side remains electrically neutral (surface charge being neutralized by the diffuse layer of counterions), the situation is qualitatively identical to the dipolar lipid model described above. In the low surface potential, limit corresponding monopole flexoelectric coefficient is easily obtainable from Eq. (5) by replacing the permanent dipole moment, μ, with the effective dipole moment of the diffuse electric double layer $\mu_D = \beta e\lambda/\varepsilon_w$, where β is the degree of ionization per lipid head. The Debye screening length λ_D gives an effective distance from the charged lipid heads to the diffuse layer of counterions.

Let us consider now the degree of ionization, β, as area dependent, $\beta(A)$. Possible reasons for a nonzero derivative, $d\beta/dA$, could be variations of the adsorption/desorption of counterions and a shift of the proton equilibrium over the membrane surfaces due to the change of the available area and/or packing-induced changes of the polar head conformation. Such conformational changes will, in turn, change the accessibility of the charged groups for protons and counterions. With respect to protons, this could be expressed in terms of a curvature-induced shift of the surface p*K*a values of the ionizable groups over the membrane surface. Bearing in mind that double layer dipoles are centerd at a distance $\lambda_D/2$ away from the membrane surface, we obtain for a blocked lipid exchange:

$$f^{CB} = \frac{e}{\varepsilon_w}\left(\frac{\beta_0}{A_0} - \left.\frac{d\beta}{dA}\right|_{A_0}\right)\lambda_D(d + \lambda_D), \tag{7}$$

where subscript 0 refers to the flat membrane state. The expression for a free lipid exchange coefficient f^{CF} is obtained by replacing d with $2\delta_H$.

Note that f^{DB} in Eq. (5) has a positive signs if μ points toward the nonpolar membrane core (the usual case found in lipid monolayers by

surface potential measurements) and that f^{CB} in Eq. (7) bears the sign of β (i.e., the sign of the surface charge). Therefore, for negatively charged lipids (the usual case with biologically relevant lipid molecules), both contributions to f (f^{D} and f^{C}) have different signs and tend to reduce each other. Since λ_D is one order of magnitude larger than the length of the permanent dipoles (ca. 1 nm at 0.1 M ionic strength), the charge contribution would be expected to be larger than the dipolar one. However, double layer dipoles are situated in a highly polar medium that is accounted for here by $\varepsilon_w \approx 30$. Therefore, the two contributions are of the same order of magnitude (Derzhanski, 1989). In fact, surface potential measurements even demonstrate that a permanent dipole contribution prevails at a lower degree of ionization. Eq. (6) permits us also to relate the sum of $f^{C} + f^{D}$ to surface potential variations. If, instead of μ we take $\mu + \mu_D$, then Eq. (6) will hold again, this time with $\Delta V = \Phi_d + \Phi_S$ (Fig. 2). Typically, in the range of 70 Å^2, $d\Delta V/dA = -6 \times 10^{17}$ V/m^2. With $d + \lambda_D = 6$ nm, we then get $f^{CB} + f^{DB} = 2.2 \times 10^{-20}$ C.

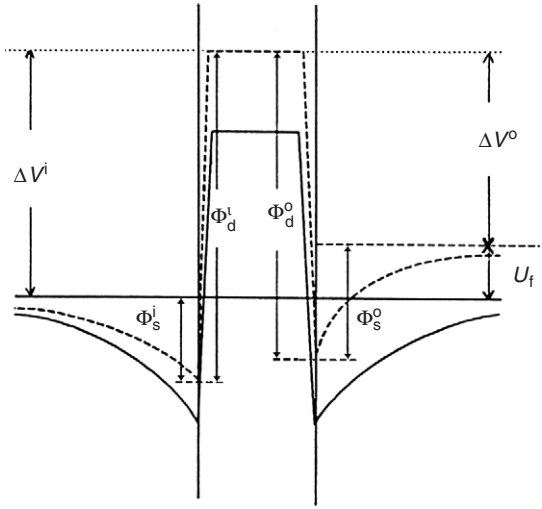

FIGURE 2 Distribution of electric potential across a flat (solid line) and a curved (broken line) bilayer lipid membrane. The membrane is composed of lipids carrying surface charge and permanent dipole. The curved potential distribution corresponds to a zero transmembrane current clamp (i.e., open circuit) measuring conditions (in other words, to zero intramembrane field). ΔV is the total monolayer surface potential (measurable in a Langmuir trough); Φ_d is the dipolar potential; Φ_S is the double layer surface potential; the superscripts i and o stand for the inner and outer monolayer, respectively. U_f is the curvature-generated (flexoelectric) potential difference. From Todorov *et al.* (1994a) with permission from the publisher.

We should note that Eq. (7) is strictly valid at low surface potentials, that is, at low partial charge per head ($\beta(\%) < 5.8/\lambda_D(\text{nm})$), when Grahame and Poisson–Boltzmann equations can be linearized. Direct calculation of the voltage difference across a spherically curved bilayer by solving the linearized Poisson–Boltzmann equation (Hristova *et al.*, 1991) confirms the validity of Eq. (7) under the additional requirement $R \gg \lambda_D$ that is always fulfilled at high enough ion concentration. The influence of the adsorption/desorption of monovalent and multivalent counterions has also been analyzed using the Langmuir adsorption model (Hristova *et al.*, 1991, 1992).

By solving the nonlinear Poisson–Boltzmann equation for charged symmetric bilayers, a self-consistent effective increase of surface charge density of the outer monolayer (and an opposite in sign decrease of the inner one) was obtained (Winterhalter and Helfrich, 1992) for a cylindrically curved bilayer (of curvature radius R) as follows (assuming that the surfaces of charges are neutral surfaces for each of the monolayers):

$$\Delta\sigma = \frac{2k_BT}{e}\varepsilon_w \frac{q-1}{p}\frac{H}{q+H}\frac{1}{R}, \tag{8}$$

where $p = \frac{\sigma e \lambda_D}{2\varepsilon_w k_B T}$, $q = \sqrt{1+p^2}$, and $H = \frac{\varepsilon_L}{\varepsilon_w}\frac{2\lambda_D}{d}$ is the electric coupling parameter. Multiplying these effective charges by the membrane thickness d, we shall obtain an expression for the area flexoelectric polarization in the nonlinear case. In the limit $p \ll 1$ and with weak electric coupling ($H \ll 1$), the resulting expression for the flexocoefficient ($f = (\varepsilon_L/\varepsilon_w)\sigma\lambda_D^2$) closely resembles the free counterpart of Eq. (7) with $\delta_H = 0$ (the surface of the charges is a neutral surface) and $d\beta/dA = 0$, apart from an additional factor of ε_L in the nominator.

b. Global Electric Neutrality. If, by curving the membrane, effective displacement of electric charges across the whole membrane thickness takes place (e.g., an excess of negative charges over the expanded outer surface and deficiency over the compressed inner surface, equivalent to an excess positive charge), this will result in a substantial electric dipole (of a length d), situated in addition in a low polar medium (ε_L). Consequently, the curvature-induced voltage difference will be large. We shall denote here the corresponding flexoelectric coefficients by f^M (monopole) in order to distinguish it from the case of detailed electric neutrality.

This effect, called a shift of surface charge equilibrium, was discussed in the general case of $\beta \neq 0$, $d\beta/dA \neq 0$ (Petrov and Sokolov, 1986), and subsequently considered from a fundamental electrostatic point of view (Derzhanski, 1989) in a special case of an area-independent degree of dissociation ($d\beta/dA = 0$). The results again depend on blocked or free lipid exchange.

The blocked one is again obtainable from Eq. (5), this time by replacing the permanent dipole moment μ with the effective dipole moment of the surface charges with respect to the bilayer's mid-surface: $-\beta ed/2\varepsilon_L$:

$$f^{MB} = -\frac{e}{\varepsilon_L}\left(\frac{\beta_0}{A_0} - \frac{d\beta}{dA}\bigg|_{A_0}\right)\frac{d^2}{2}, \tag{9}$$

while the free lipid exchange coefficient f^{MF} is obtained by replacing one $d/2$ with δ_H.

Comparing Eq. (7) with Eq. (9), we see that it holds:

$$f^M = -\frac{d}{2\lambda_D}\frac{\varepsilon_w}{\varepsilon_L}f^C = -\frac{1}{H}f^C \tag{10}$$

Consequently, the flexocoefficients for the two monopole mechanisms differ in sign and, depending on the smallness of the coupling parameter H, the difference in their magnitudes can reach about two orders, that is, $f^M \approx 1 \times 10^{-18}$ C. This clearly makes the second mechanism a leading one for the monopole case. Furthermore, estimations from monolayer measurements show that $d\beta/dA$ is making the most of the contribution. With $d\beta/dA = -5 \times 10^{18}$ m^{-2}, $d = 5 \times 10^{-9}$ m, $e = 1.6 \times 10^{-19}$ C, and $\varepsilon_L = 2$, Eq. (11) yields $f^{MB} = -5 \times 10^{-18}$ C.

Let us also note the fact that most measurements of flexocoefficients, in the presence of even a low amount of surface charge (Petrov and Sokolov, 1986; Petrov 1999), reveal these characteristically higher values. Notably, the effect of $d\beta/dA$ is clearly predominant since β/A is about -2×10^{17} m^{-2} only.

The mechanism of the shift of surface charge equilibrium implies that the excess charges emerging on the two membrane surfaces compensate each other across the membrane thickness, rather than being compensated by the diffuse double-layer counterions (Petrov and Sokolov, 1986). Indeed, if these opposite-in-sign excess charges on the two membrane surfaces were distributed continuously, the electric field created by them will be confined within the membrane capacitor.

For lipids that are both charged and dipolar, it is convenient to express the sum of two contributions to the flexocoefficient via the sum of the two components to the surface potential (Fig. 2). For Debye lengths sufficiently shorter than a half the membrane thickness, we derived a simple expression (Petrov and Sachs, 2002):

$$f^M + f^D = -\varepsilon_0 A_0 \frac{d}{2}\left(\frac{d\Delta V^i}{dA^i} + \frac{d\Delta V^o}{dA^o}\right), \tag{11}$$

where A_0 is the area per lipid molecule. In Eq. (11), the charge ($\Phi_S^{o,i}$) and dipole ($\Phi_d^{o,i}$) components of the double layer surface potential of the outer (o) and inner (i) membrane surface are lumped into one: $\Delta V^{o,i} = \Phi_S^{o,i} + \Phi_d^{o,i}$ (Fig. 2). The surface (Volta) potential ΔV is an experimentally measurable quantity in monolayers on water/air or, more representable, for half a membrane, on a water/oil interface.

Some final remarks concerning living membranes: Important feature of biomembranes is the strongly heterogeneous lipid composition of the liquid crystal membrane matrix. Studies of mixed lipid monolayers demonstrate that the variation of surface potential as a function of the area differs from those of pure monolayers: depending on the composition, $d\Delta V/dA$ can either be enhanced or weakened.

B. Flexoelectricity and Membrane Proteins

Integral proteins could provide a great contribution to the curvature-induced membrane polarization (Petrov, 1999). Both dipolar and quadrupolar contributions could be demonstrated, even more pronounced than those of the lipids. The reason for such an expectation is the very large dipole moment measured for some proteins. Theory also demonstrates that such big molecules with no spherical symmetry may have very large anisotropy of the quadrupole moment so that quadrupolar flexocoefficient f^Q can be even larger than 1×10^{-18} C.

Dipole contribution is preconditioned by free lateral diffusion of proteins. This is a basic assumption in the Singer–Nicolson fluid mosaic model of biomembranes. If a large number of conical and dipolar proteins are unidirectionally oriented, they would accumulate in the curved membrane regions, giving rise to an additional flexopolarization. Following Petrov (1999) the resulting flexocoefficient for this case is $f^{PD} = 1.6 \times 10^{-19}$ C.

Furthermore, monolayer measurements demonstrate the variations of dipole moment of peripheral proteins at stretching/compression. According to us, this implies the possibility of ''bimorph'' flexoelectricity of peripheral proteins (an analogue of the piezoelectricity of a bimorph plate), especially if these are symmetrically adsorbed over the two membrane interfaces, as suggested in the Danielli-Davson model.

The quadrupole contribution is mostly expected in membranes with high protein concentration, where ordered arrays of integral proteins do exist (Green *et al.*, 1973). Examples of this type include the inner mitochondrial membrane, the purple membranes of *Halobacterium halobium*, and so on.

IV. EXPERIMENTAL RESULTS ON FLEXOELECTRICITY IN BIOMEMBRANES

A. Theoretical Remarks

Consider a membrane whose total curvature changes in time: $c_1 + c_2 = c(t)$. According to Eq. (2) that will induce a transmembrane voltage difference, which at fast relaxation rate of the flexopolarization will follow the curvature change instantaneously: $\Delta U = (f/\varepsilon_0)c(t)$. It will also induce a displacement current in the outer circuit $I = \mathrm{d}(C_0\Delta U)/\mathrm{d}t = C_0(f/\varepsilon_0)\mathrm{d}c/\mathrm{dt}$, where C_0 is the membrane capacitance. Both effects are measurable under proper experimental conditions (see below).

Assume now a membrane shape like a spherical segment of radius R: $c_1 = c_2 = 1/R$, and membrane curvature harmonically oscillating in time: $c_1 + c_2 = c(t) = 2c_\mathrm{m} \sin \omega t$, where ω is the angular frequency of oscillations and $c_\mathrm{m} = 1/R_\mathrm{m}$ is the maximal curvature attained. Then, following Eq. (1) we shall obtain a time-dependent flexopolarization as well. This polarization leads to a transmembrane AC voltage difference [Eq. (2)] that is a first harmonic with respect to curvature oscillations and can be measured by two electrodes connected to a very high impedance electrometer (open circuit, zero current clamp). Its amplitude is $U_\mathrm{f} = (f/\varepsilon_0)2c_\mathrm{m}$.

A displacement current due to oscillating flexopolarization can also be measured by two electrodes that are effectively shorted out via low impedance ammeter (shorted circuit, zero voltage clamp). This displacement current through the meter can be calculated by adopting an equivalent circuit, containing an AC voltage generator $U_\mathrm{f} \sin \omega t$ (describing the oscillating flexoelectric voltage) and a capacitor C_0: $I_\mathrm{f} = \mathrm{d}(C_0 \cdot U)/\mathrm{d}t$. Its first harmonic amplitude is then

$$I_\mathrm{f} = C_0 U_\mathrm{f} \omega = C_0(f/\varepsilon_0)2c_\mathrm{m}\omega \tag{12}$$

In this way, measuring U_f and c_m, or I_f, C_0, and c_m, we can determine experimentally the flexocoefficient f. Evaluation of membrane curvature c_m of oscillating black lipid membranes can be performed electrically from the second harmonic of membrane capacitance current under nonzero voltage clamp (the "condenser microphone" effect) and supposing spherical curvature (Petrov and Sokolov, 1986). Actual curvature ($c_1 + c_2$) of a BLM can be measured interferometrically (Todorov *et al.*, 1991, 1994a,b), both for direct and converse flexoeffect. Patches of native membranes (see below) would need a contrast microscopic imaging under stroboscopic illumination.

B. Experimental Data

1. Direct Flexoeffect of Native Membranes at Sine Pressure Excitation

The patch-clamp method involves sealing of small patches of native membranes at the tips of glass micropipettes by gentle suction of the precleaned membrane. It is well described in the literature. Besides, a tip-dip technique was developed allowing for the formation of model phospholipid membranes on patch-clamp pipettes. Investigation of flexoelectric properties of model and native membranes (Petrov *et al.*, 1989, 1992, 1993) is a novel application of the patch-clamp technique. It is provided by the ability to manipulate the patched membrane curvature on micrometer scale by varying the pipette pressure. Theoretical analysis of the oscillating pressure technique as applied to patch-clamp was performed (Petrov and Usherwood, 1994). It was concluded that a tension-free, flaccid patch is essential for the manifestation of substantial oscillating curvature. The effect of patch tension on flexoresponse has been demonstrated (Petrov *et al.*, 1989).

Experimental setup was reported earlier (Petrov *et al.*, 1989, 1992; Petrov, 2001). The first experimental demonstration of the flexoelectric response of a native membrane from locust muscle was done in 1989 (Petrov *et al.*, 1989) using a single lock-in amplifier. Accumulation and averaging of current traces were also employed. Unlike model membranes native patches produced much noisier flexocurrents. Already at that time strong interference from channel activity of membrane patches was observed, therefore a channel-free patch may be an advantage for such measurements. Apart from the application of oscillating pressure, the membrane treatment and patching procedure closely followed the standard protocols. Patches in either cell-attached, inside-out, or outside-out configurations were studied. Tip diameters could not exceed 1 μm, though, because with larger tips gigaseal formation was precluded.

The data reported in Fig. 3 (Petrov *et al.*, 1993) were obtained using a double lock-in amplifier with an inside-out patch oscillating in the high frequency range (150–500 Hz). Oscillation frequencies were selected at which the standing waves of sound pressure were maximal at the pipette holder end of the plastic tube. Keeping the oscillating pressure amplitude constant, a linear increment of the first harmonic amplitude of 30 fA(rms)/Hz was observed. An extrapolation of the amplitude–frequency relationship passed through zero. Thus, this observation represented the displacement flexoelectric current, Eq. (12). The evaluation of membrane curvature with patches needed optical monitoring of patch geometry, because the "condenser microphone" effect is much weaker than with BLM. In the absence of such optical imaging, we could only estimate the curvature radius as equal to

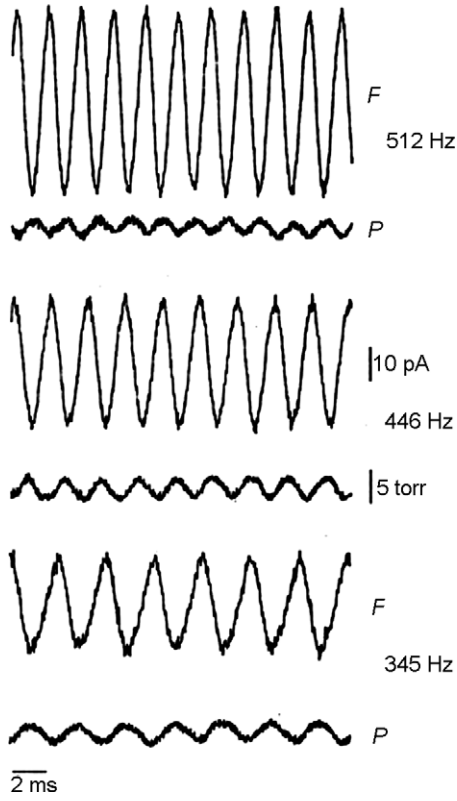

FIGURE 3 Flexoelectric recordings from an inside-out patch excised from locust muscle membrane in standard locust saline. Pipette resistance was 6.7 MΩ. Seal resistance was 0.5 GΩ. Patch capacitance components were $C_{fast} = 7.5$ pF and $C_{slow} = 0.8$ pF. Upper traces: flexoelectric response (F) of the patch at three different frequencies (345, 446, and 512 Hz) in the high frequency range. Lower traces: driving pressure signals (P). Current bar of 10 pA and pressure bar of 5 torr apply to all measurements. Flexoelectric signals were strong enough to be directly recorded from the List amplifier output. No voltage dependence of the first harmonic was observed (i.e., patch oscillated around its flat state). At 345 Hz, with 2.4 torr(pp) driving pressure a first harmonic flexoresponse of 9 pA(rms), phase $-72°$ was observed. The control pickup response after rupturing the patch and taking the pipette tip out of the saline was much lower (0.23 pA) and had a completely different phase (170°). Figure reprinted with kind permission of Springer Science and Business Media from Petrov, A. G., Miller, B. A., Hristova, K., Usherwood, P. N. R. (1993). *Eur. Biophys. J.* **22,** 289, Fig. 6. Copyright (1993) by the European Biophysical Societies' Association.

the tip radius, that is, 0.7 μm (with an error allowance of 50%). Then, we can calculate for locust muscle membrane a flexocoefficient of 2.5×10^{-18} (±50%) C, a quite substantial value (Petrov, 1999).

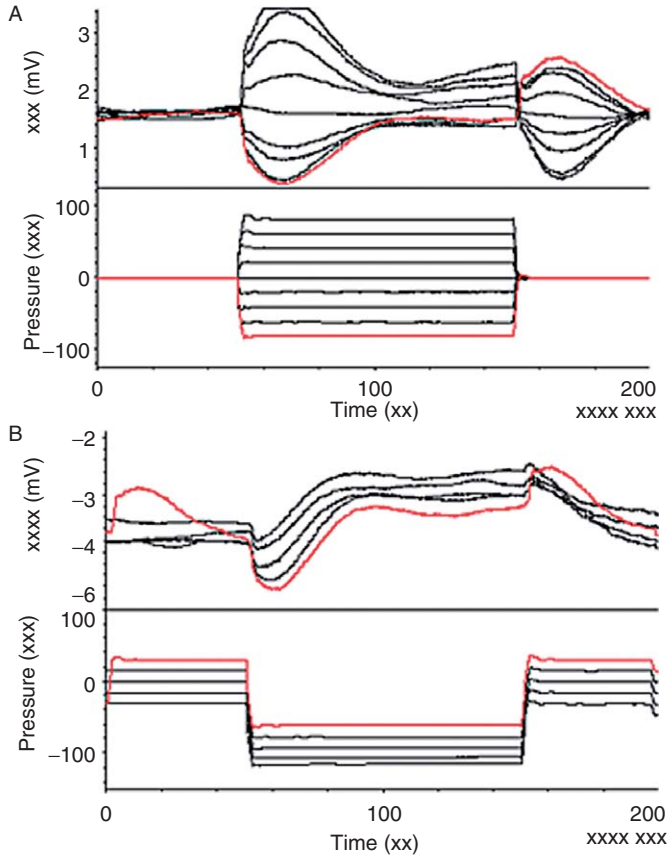

FIGURE 4 (A) Averaged voltage response of an astrocyte inside-out patch subjected to a pulse sequence of 100 ms duration which alternates between −80 and +80 torr, with averaging of corresponding traces. Patch current is clamped to zero by the regime of fast current clamp of the Axopatch 200B. Activated adult astrocytes were isolated as described in the text. An Axopatch 200B (Axon Instruments, CA) was used for patch clamping, while experimental protocols and data acquisition were controlled by Axon Instruments pClamp8 software via a Digidata 1322A acquisition system. Voltages were sampled in the regime of fast current clamp of the Axopatch 200B. All potentials are defined with respect to the pipette interior. Electrodes were pulled on a Model PC-84 pipette puller (Brown-Flaming Instruments, CA), painted with Sylgard 184 (Dow Corning Corp. Midland, MI) and fire polished. Electrodes were filled with NaCl saline (NaCl: 140 mM; KCl: 5 mM; $CaCl_2$: 2 mM; $MgCl_2$: 0.5 mM; glucose: 6 mM; and HEPES: 10 mM, pH 7.3) and had resistances ranging from 10 to 20 MΩ. Bath saline was identical to pipette-filling one. Pressure and suction were applied to the pipette by an HSPC-1 pressure clamp (ALA Scientific Instruments, NY) controlled by the pClamp software. Pressures are regarded positive and suctions negative. Up to 100 consecutive responses (voltages or currents) to various pulse protocols were collected and averaged in real time. Off-line data analysis was performed with Clampfit and Origin 6.1 software. (B) Averaged voltage response of

2. Direct Flexoeffect of Native Membranes at Pulsed Pressure Excitation

In the early studies reviewed above, oscillating pressures of various frequencies from 20 to 600 Hz have been used and the amplitude and phase of the steady AC flexoelectric response currents has been measured, using lock-in amplifiers. In contrast, transient measurements of pulse-elicited voltages and currents of membrane patches were undertaken in recent investigation. An accumulation and averaging routine of pulsed response traces was employed, the number of individually applied pulses being up to 100. A control of patch curvature was achieved by recording transients of capacitance changes (Suchyna and Sachs, 2004).

Figure 4A displays the averaged voltage response of an astrocyte inside-out patch subjected to a pulse sequence of 100-ms duration which alternates between –80 and +80 torr, with averaging of corresponding traces. Patch current is clamped to zero. Negative pressure produces negative voltage inside the pipette (head stage electrode), while positive pressure produces a positive voltage. At switching on the pulse, a rapid jump of trans-patch voltage (rise time less than 1 ms) is followed by a gradual rise resulting in a peak of 0.5–1.2 mV some 15 ms after pulse onset, dependent of pulse amplitude. Furthermore, the voltage gradually decays to roughly zero value at negative pulses in about 50 ms, while at positive value it tends to increase again after passing through a minimum. This behavior may reflect the dissipation of the voltage by a pressure-induced trans-patch current. The dependence of elicited voltage amplitude on pulse amplitude reveals an initial linear region, followed by a saturation at extreme pressures (probably due to a saturation of patch curvature, see below). At switching off the pulse, a rapid jump of trans-patch voltage (rise time less than 1 ms) of opposite sign to the switching on is followed by a mirror image of the switching on transient with respect to x-axis.

Figure 4B demonstrates the voltage response of the same patch to negative pressure pulses with constant amplitude of 80 torr, but starting from an initial value varying between +40 and –40 torr, that is, from a precurved patch state to a state of same or opposite sign of curvature. The voltage response reveals a striking dependence of the fast initial jump on the original and final sign of curvature, being minimal when both are negative and maximal when switching from negative to positive one. That is, the fast initial jump is related to a fast relaxation of patch curvature. Similar dependence is followed by the

---

an astrocyte inside-out patch to negative pressure pulses of a constant amplitude of 80 torr, but starting from an initial value varying between +40 and −40 torr, that is, from a precurved patch state to a state of same or opposite sign of curvature. Experimental conditions are the same as in Fig. 3. Current is clamped to zero by the regime of fast current clamp of the Axopatch 200B [Petrov (2006, Fig. 4) with permission from the publisher].

slow part of the response so that traces are shifted roughly parallel to one another in negative direction, while the moment of the initial peak of voltage is shifted from the 2nd to 8th s for initial pressures ranging from –40 to +40 torr. The fact that this peak time is minimum when the initial and final curvatures have the same, negative sign, reveals that the peak is related to a second, slower phase of patch curvature relaxation.

From these data, $f = (6.2 - 8.9) \times 10^{-21}$ C for rat astrocyte membrane was estimated (Petrov, 2006), which is a rather low value, but probably reasonable in view of the lack of specific electromechanical activity of such cells.

According to the interrelation of the signs of pressure and voltage difference (negative pressure producing negative voltage inside the pipette while positive pressure producing a positive voltage), the sign of rat astrocyte membrane flexocoefficient was found negative.

3. Converse Flexoeffect of Native Membranes at Sine Electric Excitation

Electrically stimulated membrane motions in cells under whole-cell voltage clamp were investigated first by using AFM (Mosbacher *et al.*, 1998). The patch pipette holding a HEK cell was attached to the tubular piezo ceramic used for x, y, z scanning. Voltage-clamped HEK293 cell membranes under AC carrier stimulus of ± 10 mV_{pp} with an AFM cantilever pressed against the membrane moved the tip some nanometer normal to the plane of the membrane. The holding potential V_h and the AC carrier voltage were applied to the cell by the patch-clamp amplifier (EPC 7). The cantilever movement was translated into a voltage, V_{det}, by the laser and quadrant detector. The output was proportional to the height difference Δh of the surface. Frequency dependence of the voltage-induced membrane movements of six HEK cells normalized to the amplitude of the lowest frequency was studied. The mean sensitivity at the lowest frequency was (0.15 ± 0.05) nm/mV_{pp} (mean $\pm$ SEM, $n = 6$) (at a cantilever stiffness of 0.01 N/m). The decrease of signal amplitude at higher frequencies was affected by the detection system (resonance frequency 2 kHz). These movements tracked the voltage at frequencies >1 kHz with a phase lead of 60°–120°, as expected of a displacement current. Tip displacement was outward with depolarization, meaning a positive sign of flexocoefficient. From the estimations made in Mosbacher *et al.* (1998), one could infer a value of 10^{-19} C for the flexocoefficient of HEK293 membrane. This value is lower than the locust muscle one, which is not surprising in view of the marked mechanoelectrical behavior of the muscle membrane.

4. Converse Flexoeffect of Native Membranes at Pulsed Electric Excitation

Further experimental results using pulsed excitation were obtained (Zhang *et al.*, 2001). Experiments were performed with whole-cell voltage-clamped HEK293 cells. The cell membrane was indented using the AFM cantilever of a

modified Quesant Nomad AFM with a force of typically 0.5 nN. For each experiment, the authors averaged 20 repetitions of the cantilever displacement associated with hyperpolarizing or depolarizing pulses (from a holding potential of –60 mV). The displacement was taken as the average of 5 ms about the peak. Positive displacements represent the AFM moving into the cell. Rectangular pulses of linearly increasing amplitude produced membrane displacements in linear proportion to the voltage pulse amplitude (~1 nm/100 mv) (Fig. 5). Hyperpolarizing the membrane would increase the local curvature around the tip as it is moving inward, that is, positive sign of the flexocoefficient of HEK293 membrane as in Mosbacher *et al.* (1998) would be confirmed at normal ionic strength. Interestingly, a sign reversal was found at lower ionic strengths of the bath, below 10 mM. It is important to note that membrane movement and ionic current were uncorrelated, suggesting the motor mechanism is not electroosmotic (cf. Fig. 5B and C).

Zhang *et al.* (2001) offered an explanation of this novel finding in terms of Lippmann equation for membrane tension in the presence of electric field.

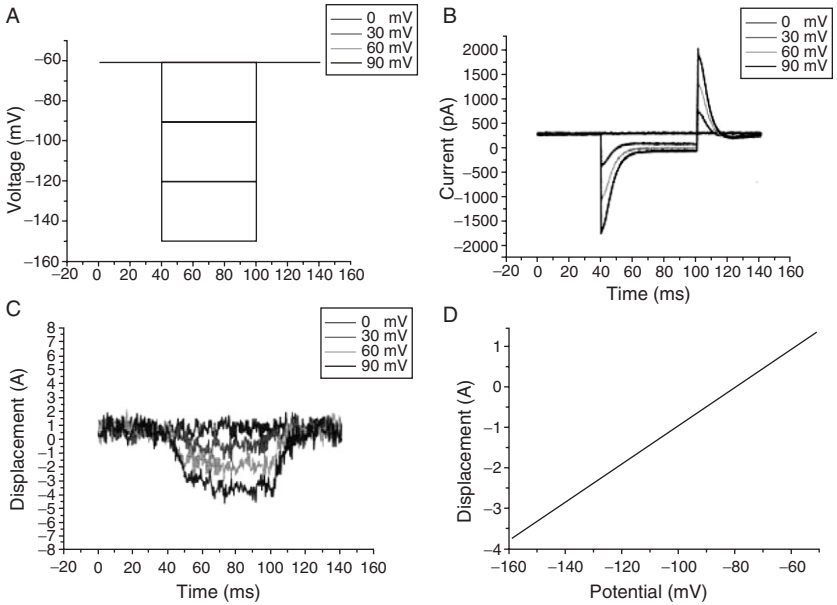

FIGURE 5 Effect of voltage on membrane movement of a patch-clamped HEK 293 cell. Steady-state displacement vs command voltage. (A)–(C) show the membrane potential, ionic current, and membrane movement from the same cell (average of 20 sweeps). (D) illustrates that the movement is linear with voltage. From Snyder *et al.* (2002, Fig. 8, p. 448) with permission from the authors and the publisher.

While in a symmetrically charged membrane Lippmann effect predicts tension changes that are quadratic with respect to transmembrane voltage, Zhang *et al.* (2001) have shown for the first time that with asymmetrically charged membranes the Lippmann tension that is a sum of the two interfacial tensions displays a leading term that is linear with respect to the voltage, thus resembling flexoelectricity.

Actually, flexoelectric torque by converse flexoeffect is roughly governed by the difference of the two interfacial tensions rather than by their sum. Such a difference will ultimately induce a surface torque that will curve the membrane. The Poisson–Boltzmann type of treatment (Zhang *et al.*, 2001) shows that this difference will also be linear with voltage, thus providing a model of the monopole contribution to the flexoeffect that depends on surface charges alone. The actual symmetry of the AFM problem is such that both tension and torque variations of the distended membrane will move the AFM tip.

5. Flexoelectricity in Channel-Containing Model and Native Membranes

Locust muscle membrane contains two types of voltage-activated channels, as found in the studies of K^+-selective channels in the membrane of adult locust muscle. The two types of K^+channels of maximum conductance ~150 pS (BK-channel) and ~35 pS (IK-channel) described by Gorczynska *et al.* (1996) were found to be also stretch-sensitive (Petrov *et al.*, 1992; Mellor *et al.*, 1999). The IK-channel displayed a monotonic reversible increase of its open probability when the transmembrane pressure was raised (Fig. 6). In contrast, during recordings from BK-channels (observed only under high K^+ concentration in the pipette), an increase of transmembrane pressure triggered the channel to its open state in an irreversible (or only slowly reversible), cumulative fashion (Fig.7).

In confirmation to the earlier results (Petrov *et al.*, 1989), we have repeatedly observed in locust, patches containing these K^+ channels that are also electrically gated, a dramatic amplification of direct flexoelectric response during channel opening (Petrov *et al.*, 1993) (Fig. 8). Channel opening was affected by applying transmembrane voltages larger than 20 mV, a property characteristic of IK channels. Increasing in a stepwise manner, the holding potential of the voltage clamp up to 50 mV we have observed, apart from the instant jumps of flexocurrent on a fast time scale (inset, 40 mV), a steady amplification of the first harmonic current amplitude of more than 50 times on the slow time scale of minutes. Initial very low flexocurrent rms value of 5 fA can be fully recovered with holding potential brought back to zero, and could be reamplified with larger negative holding potentials that also open the IK channels. This striking effect could be comprehended as a transition

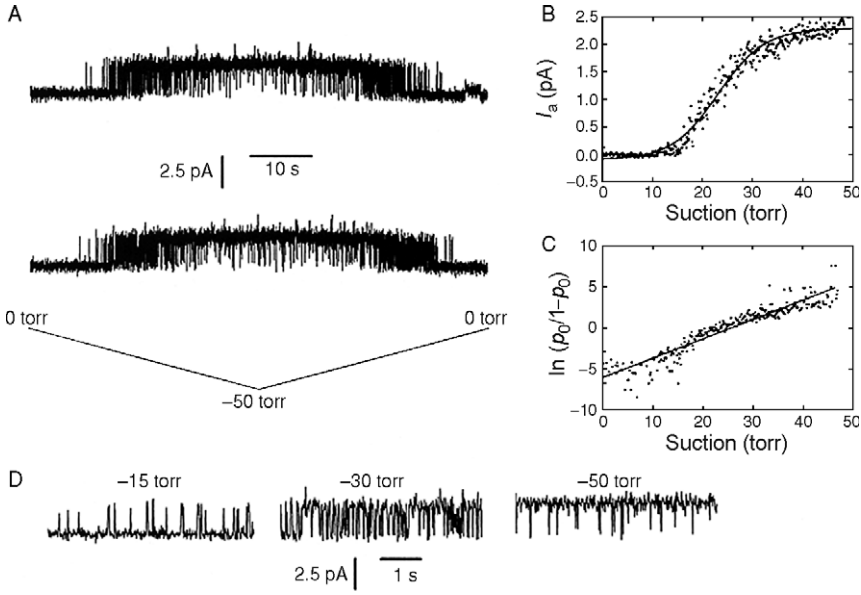

FIGURE 6 (A–D) Effect of pressure ramps on a cell-attached patch containing a single IK channel. The pipette contained low-K^+ saline and the patch was held at $V_{pip} = 70$ mV. (A) Data from two pressure ramps of "0 torr to −50 torr to 0 torr." The total duration of a ramp was 75 s, that is, the rate of change of pressure was 1.33 torr/s. There were no rest periods between the ramps. (B) Average patch current expressed as a function of pressure. Current data were sampled into 380 pressure bins (0.13 torr each) and averaged over seven rising pressure ramps (0 to −50 torr). The *solid curve* represents a fit by a Boltzmann function, with the $P_{50\%} = 23$ torr. (C) A plot of ln [p_0/(1−p_0)] vs *P*. p_0 was calculated by dividing the averaged current (Fig. 6) by the unitary channel current, $I_{unit} = 2.3$ pA. The *solid line* represents a linear regression fit to the data (slope = 0.235 ± 0.005 $torr^{-1}$, correlation coefficient = 0.94). (D) Higher time resolution traces from the rising phase of the second ramp in (A) at pressures of ~ –15, –30, and –50 torr. Figure reprinted with kind permission of Springer Science and Business Media from Mellor, I. R., Miller, B. A., Petrov, A. G., Tabarean, I., and Usherwood, P. N. R. (1999). *Eur. Biophys. J.* **28,** 346, Fig. 2. Copyright (1999) by the European Biophysical Societies' Association.

from detailed to global neutrality regime of the monopole flexopolarization during channel opening (Petrov, 1999): curvature-induced transport of charges along open channels and across the whole membrane thickness leaves each one of the half-spaces charged with respect to the other one and creates very large dipoles, situated at the same time across the low dielectric constant membrane core; therefore the enhancement of flexocoefficient can reach two orders of magnitude depending on the electric coupling parameter *H* (Petrov, 1999).

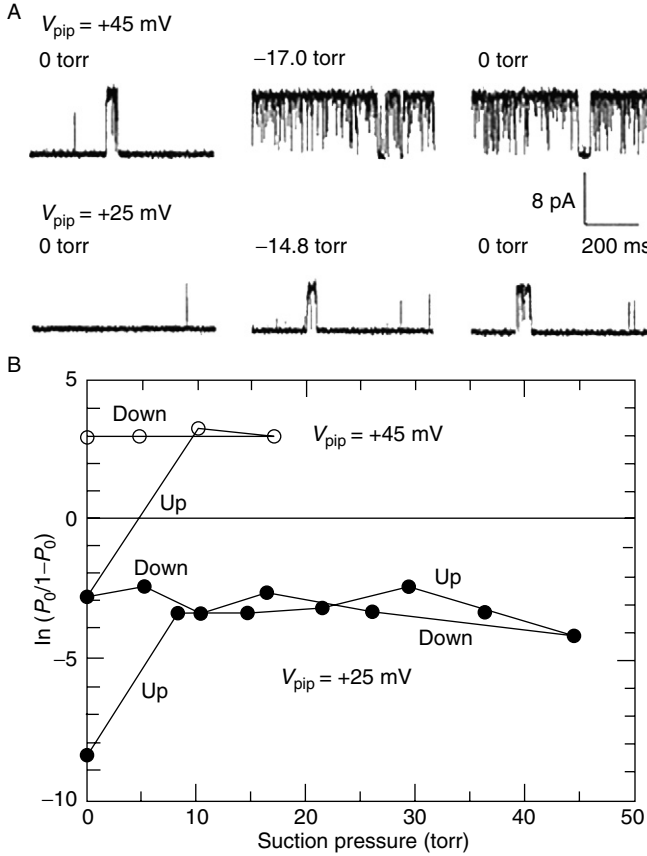

FIGURE 7 Dependence of open probability p_o of a single BK-channel on static pressure difference. Cell-attached patch, high K^+ pipette. (A) Example of current traces at $V_{pip} = +25$ and +45 mV and successive pressures of 0 torr, −14.8 (−17.0) torr, and again 0 torr. (B) Log of open probability vs pressure for the two pipette potentials following initial increase and subsequent decrease of pressure. Pressure triggers the BK-channel to activity levels, which are voltage-dependent, but no longer pressure-dependent. From Petrov (1999, Fig. 8.20) with the permission of the publisher.

Demonstration of the role of channels on the converse flexoeffect was performed by transfecting HEK cells with voltage-gated K^+ (Shaker) channels (Beyder, 2005). The voltage-induced membrane deviations' (VD) shape of the *Shaker*-transfected HEK cells (ShHEK) is notably different than the VD of wtHEK and AchR HEKs (Fig. 9). The difference can be seen as a marked nonlinearity at the point of channel activation. For both *on* and *off* steps, in the hyperpolarized portion of the VD, ShHEK membrane

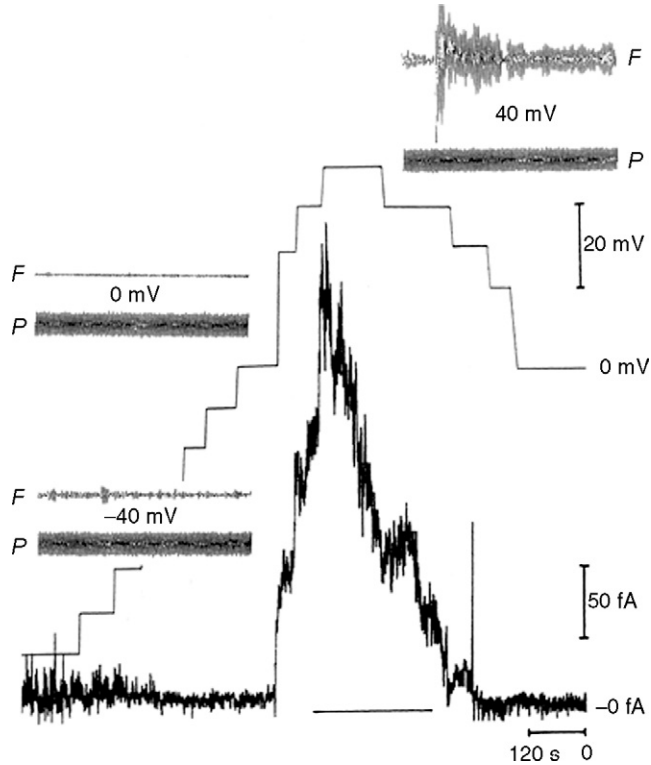

FIGURE 8 Amplification of flexocurrent (I_f) during channel opening. Cell-attached patch of locust muscle membrane. The rms amplitude of I_f (lower trace) was recorded at various values of V_{hold} (upper trace) on a slow time scale (note that time in this record runs from right to left). Direct flexoresponse was driven by pressure oscillations of 10 torr(pp), 20 Hz. Pipette resistance was 9 MΩ, seal resistance was 1 GΩ. Insets show pressure and flexocurrent in real time at indicated holding potentials. Opening of K^+ channels occurred mainly at positive holding potentials. Because of the relationship between flexopolarization and channel state, channel openings and closings could be resolved at 40 mV by sudden changes of the amplitude of flexocurrent. Figure reprinted with kind permission of Springer Science and Business Media from Petrov, A. G., Miller, B. A., Hristova, K., and Usherwood, P. N. R. (1993). *Eur. Biophys. J.* **22,** 289. Copyright (1993) by the European Biophysical Societies' Association.

displacement increases linearly with the voltage step size and the force clamp. However, from the voltage where *Shaker* channel activates (–40 to –20 mV), the VD traces for the *on* and *off* steps take a strong turn and nearly saturate in displacement (Fig. 9B). Such nonlinearity was observed in 83% (19/23) of the experiments, and the experiments lacking nonlinear behavior were performed at lowest force clamp, where mechanical noise often

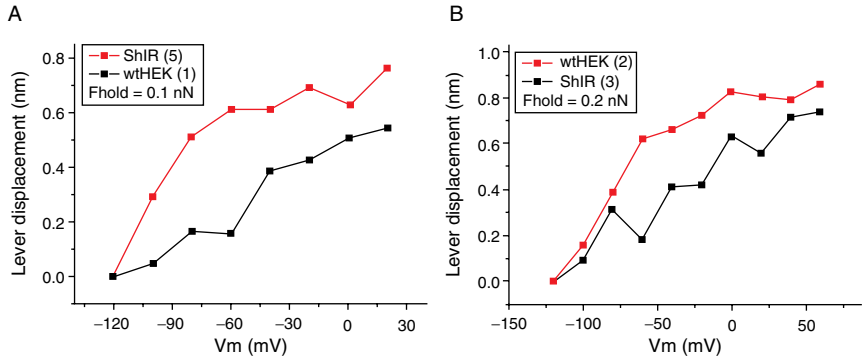

FIGURE 9 Voltage-induced membrane movements of channel-containing membranes: Shaker-transfected HEK cell (ShHEK) vs wild-type human embryonic kidney (wtHEK) cell. Movement of the cantilever engaged onto a voltage-clamped ShHEK (upper trace) was larger than movement of the cantilever engaged onto a wtHEK membrane (lower trace) for force-clamp of 100 pN (A) and 200 pN (B). Values in parentheses are the number of traces averaged. From Beyder (2005, Fig. 14, p. 49) with permission from the author.

dominates the displacement recording. This nonlinear behavior was noted at all force clamp values, down to 50 pN (Fig. 9A). This suggests that the common linear increase in movement of the cantilever drastically diminishes after the activation of *Shaker* channels.

The basic idea we offer here for explanation of these results is that open channels switch the regime of flexoelectric polarization from detailed to global electric neutrality (detailed electric neutrality: each halfspace on both sides of the membrane is neutral in itself; global electric neutrality: both halfspaces are oppositely charged with respect to one another). In the case of converse flexoeffect, detailed and global neutrality regimes should be discussed with respect to membrane-related charges only, that is, charges that are producing the electric field should not be considered. Open channels permit the transfer of charges from one side to the other, thus induced polarization could be quite large as opposite charges are separated by a large distance (membrane thickness) and by a low dielectric constant layer (hydrophobic membrane core). We have to admit in addition that a low area density of open channels will result in strict global neutrality conditions not over entire membrane area, but just over small portion of it, which will then be spread with time over the whole membrane area due to equipotentiality. However, this may be enough to explain the observed saturation (on the average) of the electric-induced curvature, in view of the fact that global flexocoefficient is some 30 times larger than the detailed one, and of opposite sign (see Petrov, 1999, Sections 6.5.1 and 6.5.2).

As Eq. (10) demonstrates, the ratio of monopole contribution at global neutrality vs monopole contribution at detailed neutrality is:

$$\frac{f^{\mathrm{MB}}}{f^{\mathrm{CB}}} = -\frac{\varepsilon_{\mathrm{w}}}{\varepsilon_{\mathrm{L}}}\,\frac{\mathrm{d}^2}{2\lambda_{\mathrm{D}}\mathrm{d}(1+\lambda_{\mathrm{D}}/d)} = -\frac{30}{2}\,\frac{5}{2\cdot 1\cdot(1+1/5)} = -\frac{150}{4.8} = -31.25$$

Closed channel:

$$f^{\mathrm{closed}} = f^{\mathrm{DB}} + f^{\mathrm{CB}}$$

Open channel: locally opposite and strong polarizations of the channels and their close surrounding area will be spread over the whole membrane area due to the equipotential condition for the electrolyte halfspace. Average flexocoefficient:

$$f^{\mathrm{open},av} = (1-\alpha)(f^{\mathrm{DB}} + f^{\mathrm{CB}}) - \alpha|f^{\mathrm{MB}}|,$$

where α is the relative portion of the area around channels per unit area. Now, since $f^{\mathrm{open},\,av} \cong 0$, it follows that $\alpha \cong 1/30$.

V. FLEXOELECTRICITY AND MECHANOTRANSDUCTION

As we have seen, flexoelectricity is a fundamental property of liquid crystals, relating their mechanical and electrical degrees of freedom. In a membrane system with just these two degrees of freedom, we can encounter flexoelectric effects discussed above, direct and converse ones. In membranes (living and model), flexoelectricity provides a linear relationship between membrane curvature and membrane polarization, or transmembrane voltage and membrane-bending stress. It is thus closely related to mechanosensitivity and mechanotransduction, basic features of all living systems.

Currently, mechanosensitivity of membranes is supposedly related to the presence of mechanosensitive channels in them. In hair cells, although no specific mechanosensitive channel has been identified, much is known about the channel's location and the cytoskeletal proteins involved in its gating and adaptation (Garcia-Añoveros and Corey, 1997; Gillespie and Walker, 2001). In particular, the channels are located at the tips of a hair cell's stereocilia, whose core filaments are composed of cross-linked actin. Extracellularly, the channels are linked by an unidentified protein or protein complex known as the tip-link, which is normally under tension; it is "prestressed," much like a tuned violin string. When the stereocilia are deflected in response to sound vibrations, the tip-link (or an associated protein at the base of the tip-link) becomes stretched, and the resulting increase in tension opens the channel.

Earlier, a different model using direct flexoelectric effect for transformation of mechanical into electrical energy in the hearing process in stereocilia was proposed (Petrov and Usherwood, 1994). Unlike mechanisms involving specialized structures like stress-activated channels, flexoelectricity may well operate in channel-free membrane regions, although its combination with ion channels brings about some interesting new possibilities (see above).

We concentrated our attention on the stereocilia tips (Fig. 10). These are highly curved membrane regions: with a stereocilium diameter of 300 nm (after Passechnik, 1988) the tip curvature $2/R$ amounts to 13×10^6 m^{-1}. During oscillations of a stereocilium in an excitatory direction, this curvature would increase because of the pull by the tip-link, respectively, decreasing in the inhibitory direction. Assuming a curvature variation of only 10% and a flexocoefficient of only 10^{-20} C, a 1.5 mV oscillation amplitude of the membrane potential may be calculated from Eq. (2) for a single stereocilium. The generation of such flexoelectric potential is concentrated in the tip region.

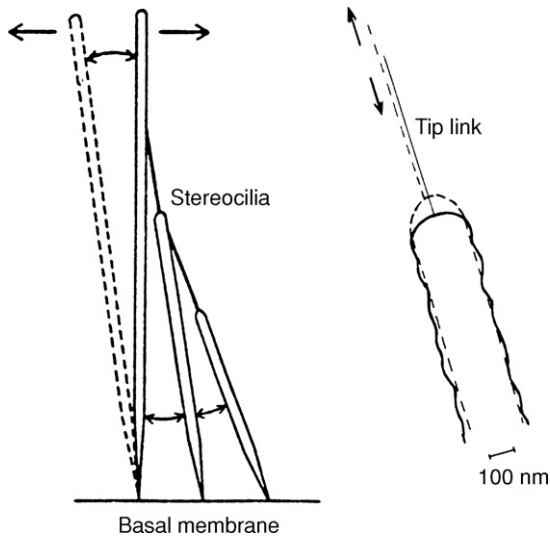

FIGURE 10 A model for applying stress to the membranes of stereocilia in hair cells. The left panel shows how tilting of the bundle of cilia to the left (excitatory excursion) leads to stretching of the membranes because of the pull by the tip-links. This observation is supposedly related to the stress-sensitive channel functioning. The right panel shows that the tip curvature under excitatory/inhibitory tilt is increased/decreased, while the cilia shaft membrane corrugation is decreased/increased. The implications of these observations in the flexoelectric sensing mechanism is discussed in the text. Figure reprinted with kind permission of Springer Science and Business Media from Petrov, A. G., and Usherwood, P. N. R. (1994). *Eur. Biophys. J.* **23,** 1, Fig. 3. Copyright (1994) by the European Biophysical Societies' Association.

There is experimental evidence that this region is the site of the mechanoelectric transducer (Hudspeth, 1982, 1983). Further, the shaft of the stereocilium membrane is corrugated at rest (Passechnik, 1988), but the folds would disappear because of the pull during excitatory excursions (Fig. 10, right). Thus, an additional source of flexoelectric potential could be recognized, with a comparable magnitude of that of the tip region, but with an opposite phase. The value of 1.5 mV favorably compares to the known values of the hair cell sensitivity of (2–4) × 105 V/m (Howard *et al.*, 1988), which yields a few millivolts change of the membrane potential at 10-nm displacement.

The flexoelectric generators of all stereocilia are in parallel, so their total e.m.f. would remain the same. However, the generated flexoelectric (displacement) current (being proportional to the membrane area) would increase in proportion to the number of stereocilia being activated in concert. With a tip area of $2\pi R = 1.4 \times 10^{-9}$ and a broadly accepted value of specific biomembrane capacity of 1 F/cm^2, the displacement current equation [Eq. (12)] gives, at 1000-Hz vibration frequency and a flexoelectric potential amplitude of 1.5 mV, a flexoelectric current amplitude of 13 fA per stereocilium, that is, 1.3 pA for a bunch of 100 stereocilia. This is a lower estimate in view of the possible additional flexoelectric current generated along the shaft of the stereocilium (see also below). The flexoelectric displacement current is of greatest interest with high frequency stimuli, when it is largest, and when its linear growth with frequency would overcome the frequency-dependent decrease in amplitude of the imposed displacement of the stereocilium. In the low frequency region, the conductive component of the current becomes important, its value being directly dependent on the conducting state of the ion channels of the stereocilium membrane (Fig. 8).

Regarding converse flexoelectric effect involvement in mechanotransduction, Petrov and Usherwood (1994) have predicted: "Thus, further exciting possibilities for the participation of flexoelectricity in the active process of mechanoamplification may be discussed, inspired in particular by the fact that the curvature-generating flexoelectric mechanism may be fast enough. By pointing out these possibilities we hope closer attention will be paid to them in future studies of the functioning of hair cells."

The converse flexoeffect into question was employed by Raphael *et al.* (2000) for description of the electromotility of outer hair cell (OHC) membrane (Fig. 11). Electromotility plays a central role in the process of mechanoamplification, which is vital for the hearing of high frequency sounds (Passechnik, 1988; Brownell *et al.*, 2001).

The OHC displays a repetitive arc and pillar nanoarchitecture, containing sharp points at the confluence of any two adjacent arcs (Fig. 11). This architecture is inherently polar and serves well the flexoelectric mechanism (e.g., a sine wave membrane shape will not do much in flexoelectric respect: while

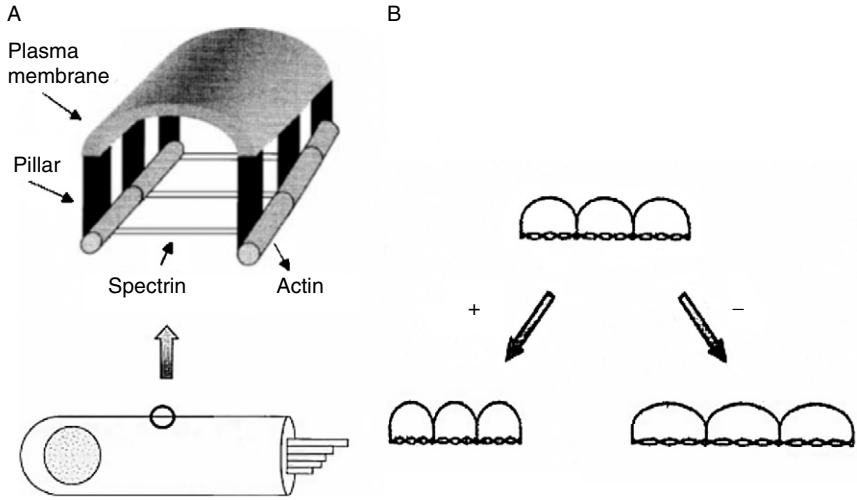

FIGURE 11 Nanomechanical model for OHC converse flexoeffect. (A) A schematic of the OHC. These cells are cylindrically shaped with lengths ranging from 20 to 90 mm along the cochlea and with a radius of 4–5 mm. The hair bundle, composed of stereocilia, is located at the apex of the cell. The lateral wall is the source of electromotility and it appears smooth under a light microscope. When examined with electron microscopy, the lateral wall appears corrugated. The folds in the membrane appear to terminate at pillar proteins that extend to the cytoskeleton. The cytoskeleton is composed of actin filaments crosslinked by spectrin molecules. (B) Curvature changes in the elemental motile unit cause extension of the spectrin molecules attached to the pillar proteins. Three units are shown in the figure. A membrane depolarization (+) leads to a decrease in the radius of curvature and a shortening of the cell while hyperpolarization (−) leads to an increase of the radius of curvature and cell lengthening. Figures reprinted with kind permission of the authors and the publisher from Raphael, R. M., Popel, A. S., and Brownell, W. E. (2000). *Biophys. J.* **78,** 2844, Fig.1 and Fig. 2. Copyright (2000) by the Biophysical Society.

one of the halfwaves is reduced the opposite one will be extended, and vice versa). Such an arc motive is repeated a few thousand times along the OHC cell membrane; this is how a *nanometer* displacement of the end of any single arc is amplified by three orders of magnitude resulting in a *micrometer* displacement of the cell end. Membrane arcs are also found in several other electromotile cells, for example, *Oscillatoria*, *Flexibacter BH3* (Brownell, 2001). This makes a membrane arc terminating on protein pillars, a basic nanoscale unit of a unique linear flexoelectric motor.

Interestingly, on a microscopic scale this motor looks like a piezoelectric one, that is, a change of cell elongation due to a change of membrane potential. Indeed, the idea that OHC possesses piezoelectric properties has been advanced by Iwasa (2001) and Dong *et al.* (2002).

However, such an apparent piezomotor features an enormously effective piezocoefficient, $c_{12} = 20{,}000{,}000 \times 10^{-12}$ C/N, which has no analogue in organic or other materials (the best piezoelectric ceramic PZT has $c_{12} = 400 \times 10^{-12}$ C/N only). We have been able to explain the apparent OHC piezoelectricity in terms of the Raphael *et al.* (2000) model, thus showing that even a very weak membrane flexoelectricity on a nanolevel, of $f = 1.10^{-21}$ C, combined with a thousand times repetition of the elemental motile unit, is capable to produce the huge apparent piezoelectricity of OHC on a microlevel (Petrov, 2003, 2006).

Brownell (2006) claims: "The fundamental motor unit in the flexoelectric based model for OHC somatic electromotility are circumferential plasma membrane ripples organized by cortical lattice F-actin. If evolution followed the suggested scenario, the ripples represent a morphed version of the stereocilium motor units of the bundle amplifier. In both cases a voltage-driven change in membrane curvature generates mechanical force. Depolarization leads to bending of the bundle toward the tallest row and to shortening of the soma. Both of which could be working in concert for the high frequency requirements of the mammalian cochlear amplifier."

One eventual consequence of this claim that would further enlarge the domain of bioflexoelectricity is to test whether ripples of muscle fiber membrane display the same pillar and arc nanoarchitecture like OHC.

VI. CONCLUSIONS

The process of mechanotransduction in membranes seems to benefit not only from specialized and localized elements like stress-activated channels, but also from the collective properties of the mechanosensitive membranes as a whole. These collective properties evolve from the liquid crystal character of membranes and are best understood in terms of liquid crystal physics (Petrov, 1999). Among them, curvature elasticity and flexoelectricity hold the first places. They ensure an effective and direct way of transformation of mechanical energy of the whole membrane into electrical one and vice versa. In doing so, both the lipid bilayer part of the membrane and the cytoskeleton of a special architecture are vital. The localized protein structures like membrane channels are obviously able to interact with global membrane properties in a striking way that is not fully understood. By confirming the existing concepts of membrane flexoelectricity in other cell types and by the eventual discovering of new concepts our exciting flexoelectric journey in the world of mechanoperception can proceed further and can reveal new important facets of the problem.

References

Beyder, A. (2005). Electro-Mechanics on the Cell Surface. Ph.D. Thesis, State University of New York at Buffalo.

Brehm, P., Kullberg, R., and Moody-Corbett, F. (1984). Properties of non-junctional acetylcholine receptor channel on innervated muscle of *Xenopus laevis*. *J. Physiol.* **350,** 631–648.

Brownell, W. E. (2001). Membrane based motor mechanisms. *In* "1st World Flexoelectric Congress." SUNY-Buffalo.

Brownell, W. E. (2006). The piezoelectric outer hair cell: Bidirectional energy conversion in membranes. *In* "Auditory Mechanisms: Processes and Models" (A. L. Nuttall, P. Gillespie, T. Ren, K. Grosh, and E. de Boer, eds.), pp. 176–186. World Scientific, Singapore.

Brownell, W. E., Spector, A. A., Raphael, R. M., and Popel, A. S. (2001). Micro- and nanomechanics of the cochlear outer hair cell. *Annu. Rev. Biomed. Eng.* **3,** 169–194.

De Gennes, P. G. (1974). "The Physics of Liquid Crystals." Clarendon Press, Oxford.

Derzhanski, A. (1989). Curvature induced polarization of bilayer lipid membrane. *Phys. Lett.* **139A,** 170–173.

Dong, X.-X., Ospeck, M., and Iwasa, K. H. (2002). Piezoelectric reciprocal relationship of the membrane motor in the cochlear outer hair cell. *Biophys. J.* **82,** 1254–1259.

Garcia-Añoveros, J., and Corey, D. P. (1997). The molecules of mechanosensation. *Annu. Rev. Neurosci.* **20,** 567–594.

Gillespie, P. G., and Walker, R. G. (2001). Molecular basis of mechanosensory transduction. *Nature* **413,** 194–202.

Gorczynska, E., Huddie, P., Miller, B., Mellor, I., Vais, H., Ramsey, R., and Usherwood, P. N. R. (1996). Potassium channels of adult locust muscle. *Pflugers Arch.* **432,** 597–606.

Green, D. E., Ji, S., and Brücker, R. F. (1973). Structure-function unitization model of biological membranes. *J. Bioenerg.* **4,** 253–284.

Guharay, F., and Sachs, F. (1984). Stretch activated single ion channel currents in tissue-cultured embryonic chick skeletal muscle. *J. Physiol.* **352,** 685–701.

Hamill, O. P. (1983). Potassium and chloride channels in red blood cells. *In* "Single Channel Recording" (B. Sakmann and E. Neher, eds.), pp. 451–471. Plenum Press, New York London.

Hamill, O. P., and Martinac, B. (2001). Molecular basis of mechanotransduction in living cells. *Physiol. Rev.* **81,** 685–740.

Howard, J., Roberts, W. M., and Hudspeth, A. J. (1988). Mechnaoelectrical transduction by hair cells. *Annu. Rev. Biophys. Biophys. Chem.* **17,** 99–124.

Hristova, K., Bivas, I., Petrov, A. G., and Derzhanski, A. (1991). Influence of the electric double layers of the membrane on the value of its flexoelectric coefficient. *Mol. Cryst. Liq. Cryst.* **200,** 71–77.

Hristova, K., Bivas, I., and Derzhanski, A. (1992). Frequency dependence of the membrane flexoelectric voltage response. Adsorption of multivalent counterions on the surface of curved lipid bilayer. *Mol. Cryst. Liq. Cryst.* **215,** 237–244.

Hudspeth, A. J. (1982). Extracellular current flow and the site of transduction by vertebrate hair cells. *J. Neurosci.* **2,** 1–10.

Hudspeth, A. J. (1983). Mechanoelectrical transduction by hair cells in the acousticolateralis sensory system. *Annu. Rev. Neurosci.* **6,** 187–215.

Ingber, D. E. (1997). Tensegrity: The architectural basis of cellular mechanotransduction. *Annu. Rev. Physiol.* **59,** 575–599.

Iwasa, K. H. (2001). A two-state piezoelectric model for outer hair cell motility. *Biophys. J.* **81,** 2495–2506.

Mellor, I. R., Miller, B. A., Petrov, A. G., Tabarean, I., and Usherwood, P. N. R. (1999). Mechanosensitive potassium channels in locust muscle membrane. *Eur. Biophys. J.* **28,** 346–350.

Meyer, R. B. (1969). Piezoelectric effects in liquid crystals. *Phys. Rev. Lett.* **22,** 918–922.
Morris, C. E. (1990). Mechanosensitive ion channels. *J. Membr. Biol.* **113,** 93–107.
Mosbacher, J., Langer, M., Horber, J. K. H., and Sachs, F. (1998). Voltage-dependent membrane displacements measured by atomic force microscopy. *J. Gen. Physiol.* **111,** 65–74.
Orr, A. W., Helmke, B. P., Blackman, B. R., and Schwartz, M. A. (2006). Mechanisms of mechanotransduction. *Dev. Cell* **10,** 11–20.
Passechnik, V. I. (1988). Mekhanizmi ulitki organa slukha. *In* "Accounts" (P. G. Kostyuk, ed.), pp. 6–121, Sci. Techn. VINITI, Moscow. *Hum. Anim. Physiol. Ser. 39.*
Petrov, A. G. (1975). Flexoelectric model of active transport. *In* "Physical and Chemical Bases of Biological Information Transfer" (J. Vassileva, ed.), pp. 111–125. Plenum Press, New York, London.
Petrov, A. G. (1999). "The Lyotropic States of Matter. Molecular Physics and Living Matter Physics." Gordon & Breach Publsisher, New York, London.
Petrov, A. G. (2001). Flexoelectricity of model and living membranes. *Biochim. Biophys. Acta* **1561,** 1–25.
Petrov, A. G. (2003). Membrane flexoelectricity at nanoscale level. *In* "2nd World Flexoelectric Congress." Rice-Houston.
Petrov, A. G. (2006). Electricity and mechanics of biomembrane systems: Flexoelectricity in living membranes. *Anal. Chim. Acta* **568,** 70–83.
Petrov, A. G., and Derzhanski, A. (1976). On some problems in the theory of elastic and flexoelectric effects in bilayer lipid membranes and biomembranes. *J. Phys. Suppl.* **37,** C3-155–C3-160.
Petrov, A. G., and Sachs, F. (2002). Flexoelectricity and elasticity of asymmetric biomembranes. *Phys. Rev. E* **65,** 021905–021910.
Petrov, A. G., and Sokolov, V. S. (1986). Curvature-electric effect in black lipid membranes. *Eur. Biophys. J.* **13,** 139–155.
Petrov, A. G., and Usherwood, P. N. R. (1994). Mechanosensitivity of cell membranes. Ion channels, lipid matrix and cytoskeleton. *Eur. Biophys. J.* **23,** 1–19.
Petrov, A. G., Seleznev, S. A., and Derzhanski, A. (1979). Principles and methods of liquid crystal physics applied to the structure and functions of biological membranes. *Acta Phys. Pol.* **A55,** 385–405.
Petrov, A. G., Ramsey, R. L., and Usherwood, P. N. R. (1989). Curvature-electric effects in artificial and natural membranes studied using patch-clamp techniques. *Eur. Biophys. J.* **17,** 13–17.
Petrov, A. G., Miller, B. A., and Usherwood, P. N. R. (1992). Mechanoelectricity of guest-host membrane systems: Lipid bilayer containing ion channels. *Mol. Cryst. Liq. Cryst.* **215,** 109–119.
Petrov, A. G., Miller, B. A., Hristova, K., and Usherwood, P. N. R. (1993). Flexoelectric effects in model and native membranes containing ion channels. *Eur. Biophys. J.* **22,** 289–300.
Raphael, R. M., Popel, A. S., and Brownell, W. E. (2000). A membrane bending model of outer hair cell electromotility. *Biophys. J.* **78,** 2844–2862.
Sachs, F. (1990). Stress-sensitive ion channels. *The Neurosciences* **2,** 49–57.
Snyder, K., Zhang, P. C., and Sachs, F. (2002). Dynamic AFM of patch clamped membranes. *In* "Ion Channel Localization Methods and Protocols" (A. Lopatin and C. G. Nichols, eds.), pp. 425–459. Humana Press Inc., Totowa, NJ.
Suchyna, TM., and Sachs, F. (2004). Dynamic regulation of mechanosensitive channels; capacitance used to monitor patch tension in real time. *Phys. Biol.* **1,** 1–18.
Todorov, A. T., Petrov, A. G., Brandt, M. O., and Fendler, J. H. (1991). Electrical and real-time stroboscopic interferometric measurements of bilayer lipid membrane flexoelectricity. *Langmuir* **7,** 3127–3137.

Todorov, A. T., Petrov, A. G., and Fendler, J. H. (1994a). Flexoelectricity of charged and dipolar BLM studied by stroboscopic interferometry. *Langmuir* **10,** 2344–2350.

Todorov, A. T., Petrov, A. G., and Fendler, J. H. (1994b). First observation of the converse flexoelectric effect in bilayer lipid membranes. *J. Phys. Chem.* **98,** 3076–3079.

Winterhalter, M., and Helfrich, W. (1992). Bending elasticity of electrically charged bilayers: Coupled monolayers, neutral surfaces, and balansing stresses. *J. Phys. Chem.* **96,** 327–330.

Zhang, P. C., Keleshian, A. M., and Sachs, F. (2001). Voltage-induced membrane movement. *Nature* **413,** 428–432.